New properties of energy-dispersed ions in the plasma sheet boundary layer observed by Cluster

A. Keiling,[1] H. Rème,[1] I. Dandouras,[1] J. M. Bosqued,[1] V. Sergeev,[2] J.-A. Sauvaud,[1] C. Jacquey,[1] B. Lavraud,[1] P. Louarn,[1] T. Moreau,[1] C. Vallat,[1] C. P. Escoubet,[3] G. K. Parks,[4] M. McCarthy,[5] E. Möbius,[6] E. Amata,[7] B. Klecker,[8] A. Korth,[9] R. Lundin,[10] P. Daly,[9] and Q.-G. Zong[11]

Received 7 October 2003; revised 17 February 2004; accepted 10 March 2004; published 18 May 2004.

[1] Using multipoint measurements from the Cluster ion spectrometry instruments and the research with adaptive particle imaging detectors, we identified new properties of multiple energy-dispersed ion structures in the plasma sheet boundary layer (PSBL). On 14 February 2001 at about 4.5 R_E midnight local time, the PSBL was highly structured, showing several large-scale dispersed ion structures, which were substructured into several (up to four) beamlets with a quasiperiodicity of 1–3 min in the spacecraft frames. The different spacecraft (SC) recorded the first dispersed ion structures at different times and on different L shells at the outer edge of the PSBL within 2 min. Three different energy dispersions were associated with the dispersed ion structures. (1) The energy dispersion of the larger-scale structures was due to the decreasing energy of individual beamlets, covering energies from 2 to >40 keV. (2) Individual beamlets of each large-scale structure showed themselves energy dispersion along the peak flux line with varying slopes, but in all cases these slopes were steeper compared to the dispersion associated with the large-scale structure. (3) A third steep energy dispersion occurred at the beginning of each beamlet and covered an energy range from a few keV to >100 keV. This dispersion was associated with recurrent impulsive acceleration processes at 11–27 R_E radial distance with a quasiperiodicity of 1–3 min. Moreover, most beamlets showed pitch angle dispersion. Superimposed on the dispersed ion structures were two transient ion injections, which had the same energy dispersion slope as described in item 3 (above), suggesting an association with the beamlets. The beamlets and one of the transient ion injections were recorded for different ion species: hydrogen, helium, and oxygen. Furthermore, echoes of beamlets were recorded, which makes this the first observation of bouncing ions in the PSBL. The echoes showed higher energy fluxes than the initial beamlets, indicating additional acceleration during subsequent current sheet crossings. Gradual thermalization of the initial beamlets after multiple current sheet crossings possibly led to the formation of the central plasma sheet. SC 1 and SC 3, longitudinally separated by only 100 km, recorded very different beamlet structures, which we interpret as a spatial effect; the two beamlet structures mapped into different magnetotail regions and underwent different spatiotemporal histories. Two possible scenarios are discussed to understand the spatiotemporal history of this highly structured PSBL. *INDEX TERMS:* 2748 Magnetospheric Physics: Magnetotail boundary layers; 2764 Magnetospheric Physics: Plasma sheet; 2720 Magnetospheric Physics: Energetic particles, trapped; 2744 Magnetospheric Physics: Magnetotail; *KEYWORDS:* energy-dispersed ions, beamlet, PSBL, Cluster spacecraft, bouncing ion cluster

[1]Centre d'Étude Spatiale des Rayonnements, Centre National de la Recherche Scientifique, Toulouse, France.
[2]Institute of Physics, St. Petersburg State University, St. Petersburg, Russia.
[3]Research and Scientific Support Department, European Space Agency/European Space Research and Technology Centre, Noordwijk, Netherlands.
[4]Space Science Laboratory, University of California, Berkeley, California, USA.
[5]Department of Geophysics, University of Washington, Seattle, Washington, USA.
[6]Space Science Center, Institute for the Study of Earth, Oceans, and Space, University of New Hampshire, Durham, New Hampshire, USA.
[7]Istituto di Fisica dello Spazio Interplanetario, Consiglio Nazionale delle Ricerche, Rome, Italy.
[8]Max-Planck-Institut für Extraterrestrische Physik, Garching, Germany.
[9]Max-Planck-Institut für Aeronomie, Katlenburg-Lindau, Germany.
[10]Swedish Institute of Space Physics, Kiruna, Sweden.
[11]Center for Space Physics, Boston University, Boston, Massachusetts, USA.

0148-0227/04/2003JA010277

Citation: Keiling, A., et al. (2004), New properties of energy-dispersed ions in the plasma sheet boundary layer observed by Cluster, *J. Geophys. Res.*, *109*, A05215, doi:10.1029/2003JA010277.

1. Introduction

[2] Energy-dispersed ion structures (EDIS) are well-known ion signatures in the magnetosphere. These ion structures show a monotonic decrease in energy as a function of either time or decreasing latitude depending on their type. In Figure 1 we sketch the three main types reported in the literature: velocity-dispersed ion structures (VDIS) (note that the usage of this term is not consistent in the literature), time-dispersed ion structures (TDIS), and intrinsically dispersed ion structures (IDIS). Various generation mechanisms have been proposed for the different types, among which are inverted Vs above the ionosphere [*Bosqued et al.*, 1986], inductive electric fields in the equatorial near-Earth tail [*Quinn and Southwood*, 1982], neutral sheet acceleration [*Lyons and Speiser*, 1982] and reconnection [*Cowley*, 1980] in the magnetotail, resonant kinetic Alfvén waves in the plasma sheet boundary layer (PSBL) [*Hasegawa*, 1987], and fast mode waves in the dayside magnetosphere [e.g., *Boehm et al.*, 1999]. These mechanisms differ greatly in their physical properties. Only in exceptional cases can acceleration processes be observed in situ, and therefore most acceleration mechanisms in the magnetosphere are still speculative.

[3] In spite of many years of research the role of EDIS in magnetotail dynamics and in auroral physics is not conclusively established, although it has been suggested that they contribute to creating the aurora [e.g., *Kan and Akasofu*, 1976; *Lyons and Evans*, 1984] and also to the formation of the central plasma sheet (CPS) [e.g., *Lyons and Speiser*, 1982]. In recent observational studies, EDIS observed in the magnetotail have been directly associated with ionospheric and plasma sheet (PS) activities [*Elphinstone et al.*, 1995; *Sauvaud et al.*, 1999; *Sergeev et al.*, 2000; *Kazama and Mukai*, 2003]. Furthermore, it appears that different types of EDIS in the magnetotail are observed during different substorm phases. Whereas TDIS have been mostly associated with the expansion phase [*Sauvaud et al.*, 1999; *Sergeev et al.*, 2000], VDIS and IDIS have often been associated with the recovery phase [*Zelenyi et al.*, 1990; *Bosqued et al.*, 1993; *Elphinstone et al.*, 1995]. This suggests that different generation mechanisms operate at different times in the magnetotail.

[4] Earlier studies have shown that some EDIS in the auroral zone and the PSBL consist of smaller-scale structures [*Takahashi and Hones*, 1988; *Bosqued et al.*, 1993]. Particle simulations by *Ashour-Abdalla et al.* [1992] reproduced the small-scale structures, which were coined beamlets. According to their model, plasma mantle ions convecting into the magnetotail current sheet find themselves in an alternating pattern of enhanced trapping and ejection. The amount of acceleration within the current sheet is a function of the magnetic field component perpendicular to the current sheet [*Zelenyi et al.*, 1990]. The accelerated and ejected ion beams follow Speiser orbits [*Speiser*, 1967], form the PSBL, and give the EDIS its peculiar beamlet structure in the Ashour-Abdalla et al. simulation. Although experimental evidence for this physical property (beamlet structure) exists, the information obtained from the observations is limited.

[5] Using multipoint measurements from the Cluster fleet, we have investigated multiple energy-dispersed ion structures in the PSBL at geocentric distances of 4–6 R_E. Here we present one event (14 February 2001) in detail. In particular, we show observations of the fine structures (beamlets) of the dispersed ion structures and discuss their origin. New properties of EDIS and beamlets are identified which extend the current view on ion beams in the PSBL.

2. Instrumentation

[6] The observations presented here are from three Cluster spacecraft (SC) (SC 1, SC 3, and SC 4). The Cluster fleet is placed in a 57-hour orbit with a perigee and an apogee of 4 and 19.6 R_E geocentric distance, respectively. Data from the Cluster Ion Spectrometry (CIS) instruments [*Rème et al.*, 2001] and the Research with Adaptive Particle Imaging Detectors (RAPID) [*Wilken et al.*, 1995] were used in this study.

[7] Each CIS instrument has two complementary sensors to measure the full, three-dimensional (3-D) ion distributions with a time resolution of up to 4 s (one spin period). The composition and distribution function (CODIF) analyzer measures the distribution of H^+, He^+, He^{++}, and O^+ in the energy range from ~0 to 40 keV with an angular resolution of 22.5°. The hot ion analyzer (HIA) does not offer mass resolution but has a better angular resolution of 5.6° and an energy range up to 34 keV.

[8] RAPID is a particle detector for the analysis of plasma distributions in the energy range from 30 to 1500 keV for H^+ and from 10 to 1500 keV nucleon^{-1} for He^+ and O^+ with a time resolution of up to 4 s (one spin period). In addition to the Cluster data we utilized ground magnetic field data from the International Monitor for Auroral Geomagnetic Effects (IMAGE) and auroral images from the wideband imaging camera of the far-ultraviolet imaging instrument on board the IMAGE spacecraft [*Mende et al.*, 2000].

3. Observations

3.1. Overview

[9] We have visually inspected CIS data for about 90 perigee (4–6 R_E) lobe-PSBL crossings. A rich phenomenology was found. Several crossings showed signatures of ion energy dispersion of which the clearest examples were found for inbound passes. The event presented in this study was chosen because of its complexity and its clearly visible fine structure allowing us to determine new properties. In addition, the separation between the satellites was small (500–900 km) and thus favorable for the investigation of spatial and temporal aspects.

[10] On 14 February 2001, multiple energy-dispersed ion structures were recorded in the PSBL by the Cluster spacecraft while on an inbound orbit (Figure 2). At ~0045 UT (0.1 MLT, 4.5 R_E, and −70° invariant latitude (ILAT)), SC 1 crossed the lobe-PSBL interface first. The

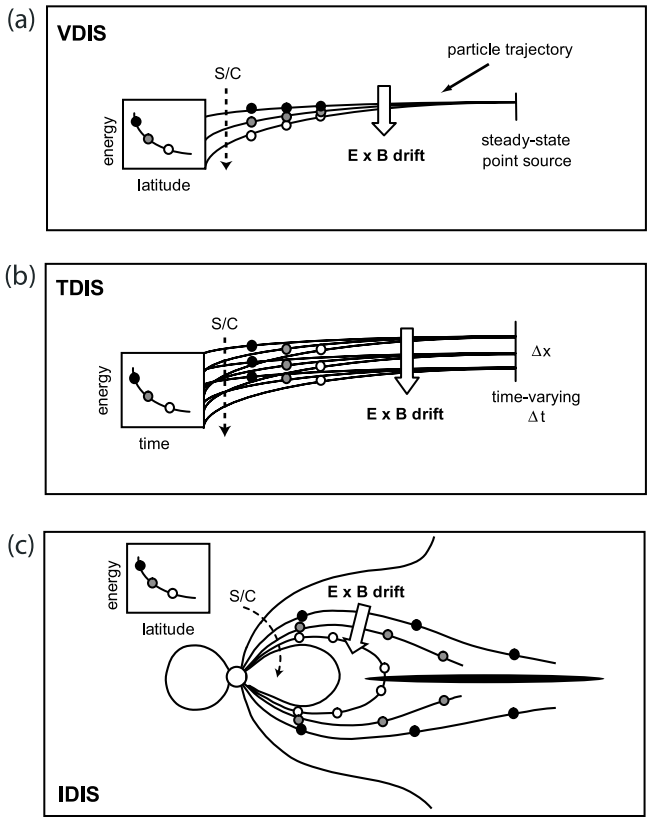

Figure 1. Three types of dispersed ion structures. (a) Velocity-dispersed ion structure (VDIS). A pointlike source continuously ejects ions onto magnetic field lines. Owing to the equatorward **E** × **B** drift the ions are dispersed along latitude; faster ions reach the spacecraft at higher latitude. The observed dispersion is entirely due to the **E** × **B** drift. Although all three types of dispersions (described here) show an ion velocity dependence, it is this type which is commonly referred to as VDIS. (b) Time-dispersed ion structure (TDIS). Ions are ejected from a spatially extended source. The injection time is short. The dispersion is caused by the different travel times it takes ions with different energies to reach the spacecraft. Thus the dispersion is a function of time. Whether the satellite crosses L shells or not during the observations plays no role. Note that the source can be point-like which, however, makes it unlikely to record the entire ion dispersion signature by the spacecraft. (c) Intrinsically dispersed ion structure (IDIS). Neither **E** × **B** drift nor time-of-flight effect plays the key role. The dispersion is caused at the source in contrast to the previous two types which require the ions to travel a certain distance for the dispersion to appear. For IDIS the source is distributed along the magnetotail covering a range of L values. Depending on the magnetic field component perpendicular to the current sheet, ions with different energies are ejected. The dispersion pattern is a function of latitude.

GSE locations of SC 1 and SC 4 relative to SC 3 at the time of the PSBL entry by SC 1 are also shown.

[11] CIS-HIA ion energy-time spectrograms of SC 1 and SC 3 show two (A, B) and three (A, B, C) extended dispersed ion structures, respectively (Figure 3). Note that the labels A, B, and C will be used consistently throughout this paper denoting the same order of these ion structures, even though these structures are not necessarily the same physical entities at all three spacecraft. The first dispersed ion structure of both spacecraft constitutes the entry into the ion PSBL coming from the lobe. The lobe-PSBL interface was encountered at different times and on different L shells by the three spacecraft. This will be shown, and its implication will be discussed in section 3.2. The larger-scale dispersed ion structures show substructures, seen particularly well in SC 1, which we call beamlets in accordance with *Ashour-Abdalla et al.* [1992]. Section 3.3 will present the properties of these beamlets, whereas the cause of the beamlet structure will be discussed in section 4. Whether the second (B) and third (C) dispersed ion structures are new ion injections or simply echoes of the first (A) dispersed ion structure will be the focus of section 3.4.

[12] At 0046 and 0055 UT, two additional dispersed ion structures (labeled "d" and "e" in Figure 3) were recorded by SC 1. In section 3.5 we will show how these temporal structures are related to the beamlets of the larger structures, A and B. This PSBL crossing is accompanied by transient low-energy ion outflows from the ionosphere (Figure 3), which we will not discuss in this paper.

[13] The entire spacecraft crossing of the dispersed ion structures took about 15 min. This region is the ion PSBL, which, by definition, is associated with ion beams [*Parks et al.*, 1984; *Eastman et al.*, 1984]. Following the PSBL is a less structured, thermalized ion population, which, by definition, is the CPS [*Frank et al.*, 1976; *Eastman et al.*,

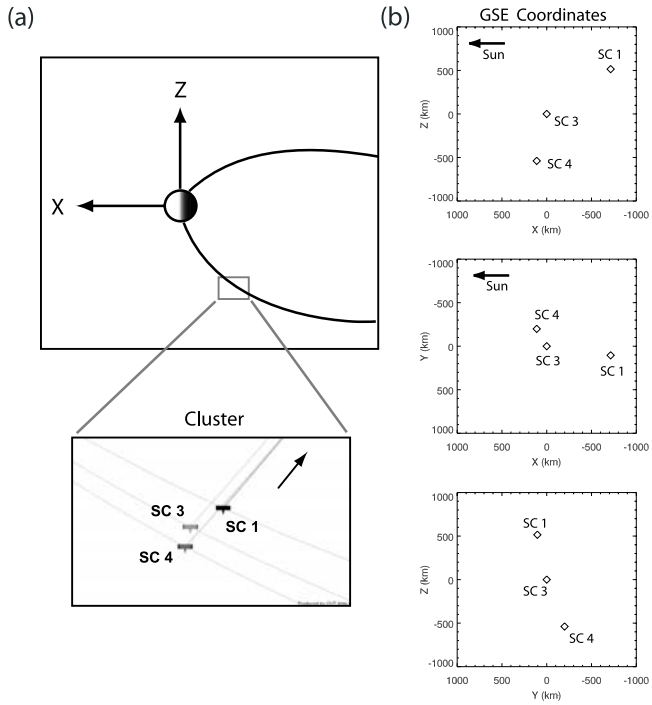

Figure 2. (a) Partial Cluster orbit and spacecraft configuration on 14 February 2001 at 0045 UT (Orbit Visualization Tool, available at http://ovt.irfu.se). SC 2 is not shown. (b) Spacecraft locations relative to SC 3 in GSE coordinates at 0045 UT.

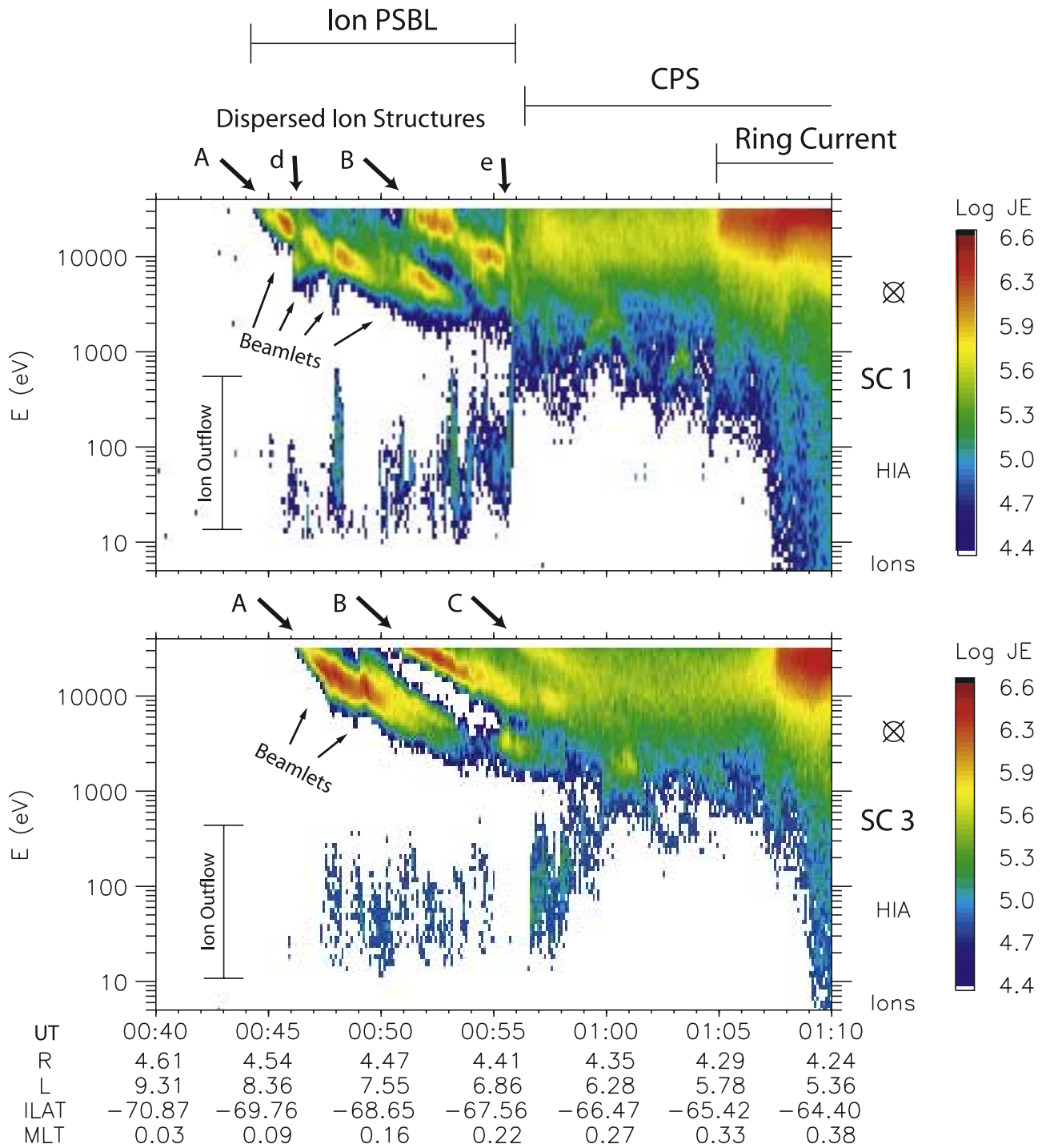

Figure 3. Overview of the ion measurements from SC 1 and SC 3 during the lobe- PSBL crossing on 14 February 2001, showing energy-time spectrograms of ions (CIS-HIA). The ephemeris data correspond to SC 3. Various structures are pointed out: dispersed ion structures (A, B, C, d, and e), ion outflows, ring current, PSBL, and the central plasma sheet. The main focus of this paper is the dispersed ion structures and their substructures (beamlets), seen particularly well on SC 1.

1984]. At 0105 and 0107 UT, SC 1 and SC 3, respectively, encountered the outer edge of the ring current.

[14] Geomagnetic activity during the lobe-PSBL crossing was disturbed: Kp = 4−, AE = 326 nT (averaged). Nevertheless, the substorm recovery phase prevailed according to some auroral stations (NAL, LYR, HOR, BJN) of the IMAGE ground magnetometer network (Figure 4). According to lower-latitude stations (MUO, PEL) the event also occurred during the recovery phase of an intensification. At the same time, ultraviolet images from the IMAGE satellite show a double oval (Figure 5), which is a typical recovery phase signature [*Elphinstone et al.*, 1993]. The footprints of

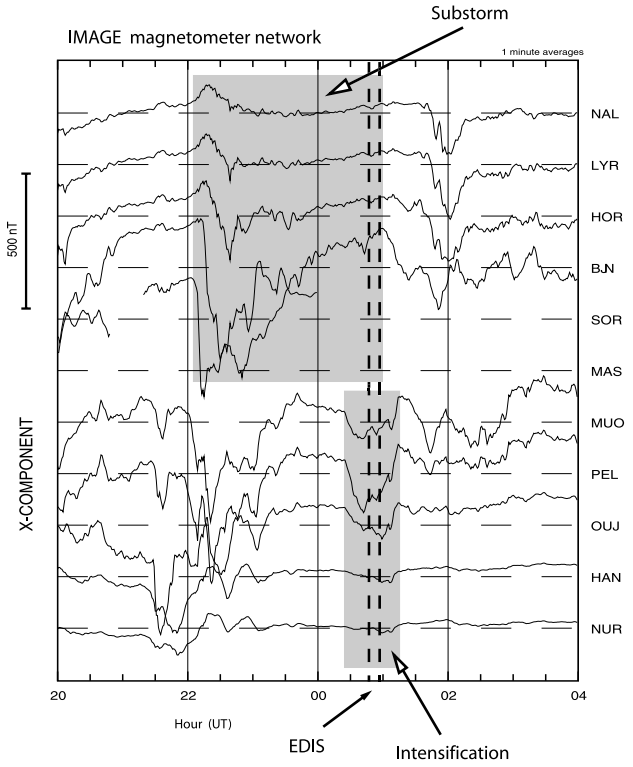

Figure 4. The x component of ground magnetic field data on 14 February 2001. The shaded areas indicate a substorm and an intensification around the time the dispersed ion structures were encountered by Cluster. Dashed lines mark the beginning and the end of the ion structures.

the Cluster spacecraft, mapped into the Northern Hemisphere ionosphere, are indicated by a circle. The Cluster spacecraft were magnetically conjugate to a small activated region in the poleward oval of the double oval. At ~0054 UT, auroral activity increased on the dusk side. This activity did not reach the area where Cluster's footprints were, as also seen in later images (not shown).

3.2. Spatial and Temporal Characteristics

[15] In this section we investigate some spatial and temporal characteristics of the dispersed ion structures by using measurements from three Cluster spacecraft. At the same time, we want to establish whether or not the ion structures observed by the different spacecraft were the same. The data used in this section come from the CODIF analyzers (16-s time resolution), which were operational on the three spacecraft (HIA was not operational on SC 2 and SC 4). In this section we will not discuss specific properties of the small-scale structures (beamlets) of the dispersed ion structures, which will be done in section 3.3 using higher-time resolution data from HIA (4-s time resolution).

[16] Figures 6a–6c show energy-time spectrograms of H^+. The three spacecraft encountered the first (outermost) dispersed structure at different times (indicated by vertical dashed lines). The time delays were ~1.5 min between SC 1 and SC 3 and ~0.5 min between SC 3 and SC 4. The structures were observed for ~1 min at fixed energy level in each spacecraft frame. The ion structures recorded by SC 1 were very different from those recorded by SC 3 and SC 4. The comparison between SC 3 and SC 4 is more complicated. The first dispersed ion structure, structure A, recorded by SC 3 consisted of two beamlets between 0046 and 0050 UT (Figure 6b). Although there is only a vague indication of a second beamlet (see black line in Figure 6b), this beamlet and additional ones are visible in the higher-resolution data (Figure 7 of section 3.3). Similarly, one might argue that structure A, recorded by SC 4 (Figure 6c), consisted of two beamlets between 0047 and 0050 UT because of the similarity with structure A of SC 3. (Note that the energy scales in Figures 6b and 6c were chosen differently to compensate for the smaller energy flux recorded by SC 3.) Further, it appears as if the second beamlets recorded by both spacecraft started at the same time (see black line). As we will show below, both beamlets were recorded on field lines with different L values (see solid white lines in Figures 6e and 6f), which suggests that a temporal process created these beamlets.

[17] Looking at the second ion structure (B) on all three spacecraft, we note the following (Figures 6a, 6b, and 6c): Structure B was encountered by SC 3 before it was encountered by SC 1, which is the reverse order compared to the first ion structure (A). This again shows that SC 1 and SC 3 observed different structures. Note also that this resulted in a longer time separation between the first (A) and the second (B) structure for SC 1 and SC 3. On the other hand, SC 1 and SC 4 observed the second ion structure quasi-simultaneously. Since the spacecraft were spatially separated (i.e., the structures were encountered on

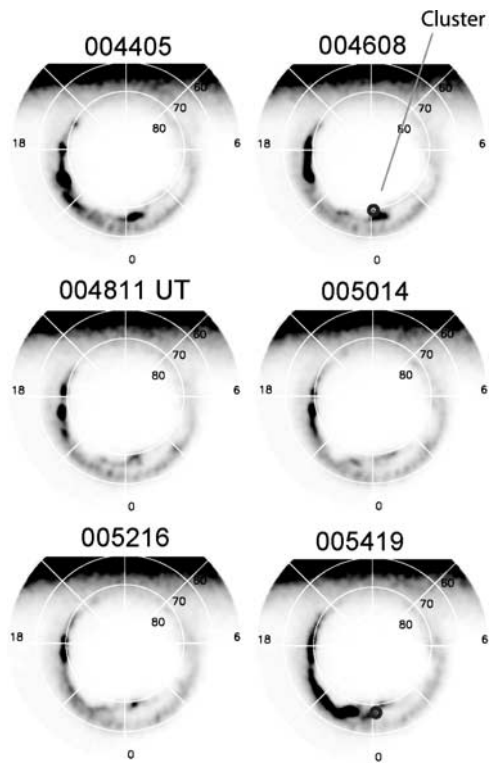

Figure 5. Far-ultraviolet images from the wideband imaging camera on board the International Monitor for Auroral Geomagnetic Effects spacecraft showing a double oval in the Northern Hemisphere. Cluster's footprints (circles) were mapped using Tsyganenko T89.

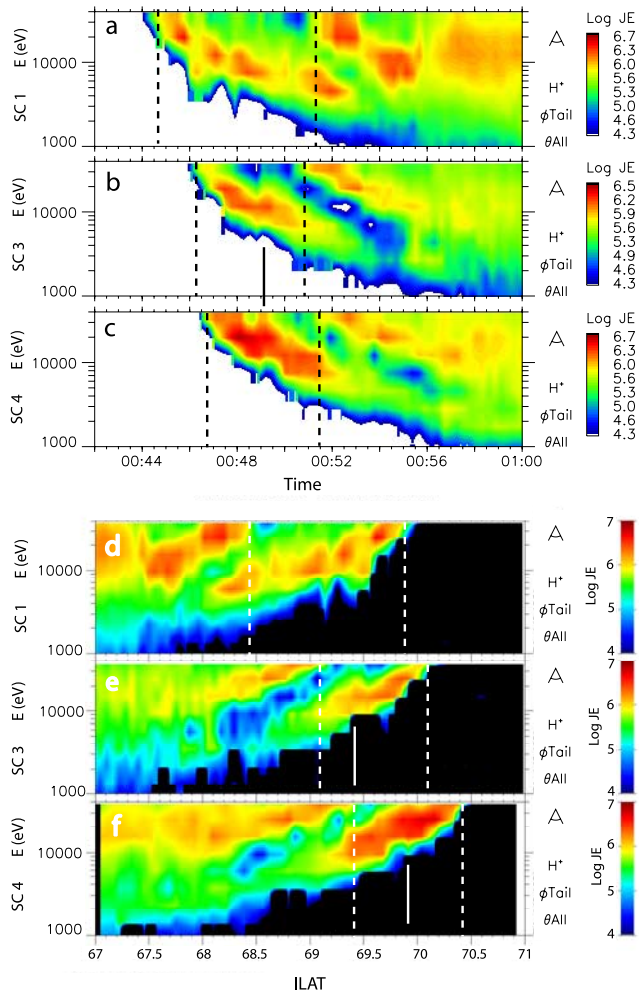

Figure 6. Energy-dispersed ion structures recorded by CIS-Composition and Distribution Function (CODIF) on SC 1, 3, and 4 during the PSBL crossing on 14 February 2001. (a–c) Energy-time spectrograms of hydrogen ions. (d–f) Energy-latitude spectrograms of hydrogen ions. The L values were determined using the Tsyganenko T89 magnetic field model. The look direction of the instruments was tailward. The time resolution is 12 s.

different L shells (Figures 6d and 6f)), it can be argued that a temporal structure covering a larger range of L shells was simultaneously recorded by both spacecraft. However, the fine structure (beamlets) at SC 1 is very different from the fine structure at SC 4, and hence this quasi-simultaneous occurrence is a coincidence. In fact, in section 3.4 we will argue that the B structures of all spacecraft are echoes of the preceding A structures.

[18] The time delay between the encounters of the second ion structures (B) by SC 3 and SC 4 was ~0.5 min, which is approximately the same as the time delay of the encounters of the first ion structures (A). This suggests that very similar injections were observed by both spacecraft, both with the same time delay for the echoes (B structure). We also showed that the A structures of SC 3 and SC 4 were similar. However, when comparing the B structures on SC 3 and SC 4, we notice more differences. The beamlets did not occur at the same time nor were they time shifted by a constant delay. The overall dispersion slope and duration of these structures are very similar, nevertheless. Different fine structure of structure B between SC 3 and SC 4 and different injection locations (L values) of structure A (see next paragraph) lead us to conclude that the two spacecraft recorded different ion structures or at least structures with different spatiotemporal histories.

[19] In addition to the different observation times of the ion structures (A and B) by the three spacecraft, the energy-latitude spectrograms (Figures 6d–6f) show that the first (outermost) ion structures were encountered on different L shells by the three spacecraft, indicating that the lobe-PSBL interface was relocated outward. This interpretation is supported by far-ultraviolet (FUV) images that show a poleward expansion by ~1.5° of the poleward boundary of the oval (Figure 5). An upper limit estimate (using time delay measurements) yields an outward motion of the in situ lobe-PSBL interface of 5 and 20 km s^{-1} during the encounters of this interface by SC 1 and SC 3 and by SC 3 and SC 4, respectively. Encounters of the ion structures on increasing L values suggest that ions were injected at locations with increasing distances from Earth. A possible scenario for the differences in time and latitude of the spacecraft encounters with the structures is an ion source, located at or away from an X line, that retreats with the retreating X line. A retreating X line is also consistent with the recovery phase that prevailed during this event. The closeness of the outermost ion structure to the lobe-PSBL interface and the retreating source during recovery implies that the ion source of the outermost structure was likely located beyond 30 R_E and probably much farther. The scenario of a tailward moving source has been described by *Forbes et al.* [1981] and *Andrews et al.* [1981], and it was argued that a tailward moving source and the equatorward $\mathbf{E} \times \mathbf{B}$ drift can account for dispersion in the plasma sheet boundary [*Andrews et al.*, 1981].

[20] The fact that SC 1 encountered very different ion structures compared to those encountered by SC 3 and SC 4 is most likely due to the longitudinal separations of the three spacecraft. SC 1 was separated in the y (GSE) direction by ~100 km from SC 3 and by ~300 km from SC 4 when crossing the lobe-PSBL interface (Figure 2). In comparison, the ion gyroradius for particles with perpendicular velocity $v_\perp = 2000$ km s^{-1} (H^+) at Cluster's location was about 45 km. Since the different PSBL locations of the ion structures were magnetically connected to different regions in the magnetotail, it is possible that each source region ejected ions that underwent different spatiotemporal histories. Without knowing the distance of the source regions away from Earth, it is not possible to reliably estimate their longitudinal separation in the far tail. In section 3.5 we will show evidence for transient ion injections on SC 1, not seen on SC 3 or SC 4, which supports the case that the differences between SC 1 and both SC 3 and SC 4 are indeed due to their longitudinal separations. The differences between SC 3 and SC 4 can be explained similarly.

[21] We summarize this section as follows: (1) The three spacecraft recorded different ion structures. (2) The outermost ion structures recorded by different spacecraft were

injected on field lines with increasing L values, i.e., from regions progressively farther away in the magnetotail, and this source region is most likely located beyond 30 R_E radial distance. (3) The retreating ion source implies a temporal component in the generation of the ion structures. (4) The ion structures recorded by SC 1 and SC 3 were independently ejected from azimuthally separated regions in the far magnetotail. (5) It was shown to be possible that the beamlet structure of the large-scale structure A on both SC 3 and SC 4 could have been created by a temporal process. Additional evidence for spatial and temporal effects will be given in section 3.3. (6) The lobe-PSBL interface expanded poleward with velocities of 5–20 km s^{-1} (upper limit estimates).

3.3. Substructure: Beamlets

[22] We now draw attention to the smaller features (beamlets) inside the large-scale dispersed ion structures which were labeled A, B, and C in Figure 3. Beamlets are defined here as ion structures with energy fluxes (JE) greater than ~5.6 on the logarithmic scale in Figures 7b and 7d. We describe properties such as energy range, pitch angle, composition, dispersion slopes, and some temporal and spatial aspects.

3.3.1. Energy Range of Beamlets

[23] Figure 7 shows an expanded time interval of the PSBL crossing on 14 February 2001 for SC 1 and SC 3. We combined energy-time spectrograms from CIS and RAPID covering an energy range from 1 to 1500 keV. CIS-HIA data of SC 1 (Figure 7b) reveal four beamlets (A1–A4) constituting the first ion structure (A); the second ion structure (B) contains two distinct beamlets (B1 and B2). For SC 3 (Figure 7d), three distinct beamlets (A1, A2, and A4) and possibly a fourth one (A3) were embedded in the first structure, and three beamlets (B1, B2, and B3) were embedded in the second structure, noting that the separation between B2 and B3 is not as clear. Additionally, SC 3 recorded a third dispersed structure with only one beamlet (C1, better seen in Figure 3). The durations of both the individual beamlets and the gaps between beamlets varied in the spacecraft frame. A beamlet structure is also visible in the RAPID data for H^+ with >30 keV (Figures 7a and 7c), and individual beamlets correspond to the beamlets recorded by CIS (indicated by vertical dashed lines). We emphasize that this means that not only the first beamlet of each large-scale structure (A1, B1, and C1) but in fact each beamlet was associated with very high energies (>30 keV) in addition to the energies at peak fluxes (<30 keV). This surprising result leads to a separate energy dispersion which will be investigated more in section 3.3.3.

[24] To determine the upper energy threshold of the beamlets more precisely, we show differential flux versus time for different energy channels in Figure 8. Beamlet structures can be seen more or less well developed in energy channels of up to 170 keV for hydrogen. Some oxygen and helium beamlets are also present with a species-dependent time delay with respect to the hydrogen beamlets. We also note that whereas for SC 1 the first hydrogen beamlet (A1) was clearly present in higher energy channels (>30 keV), SC 3 only recorded the first beamlet in the 30 keV energy channel.

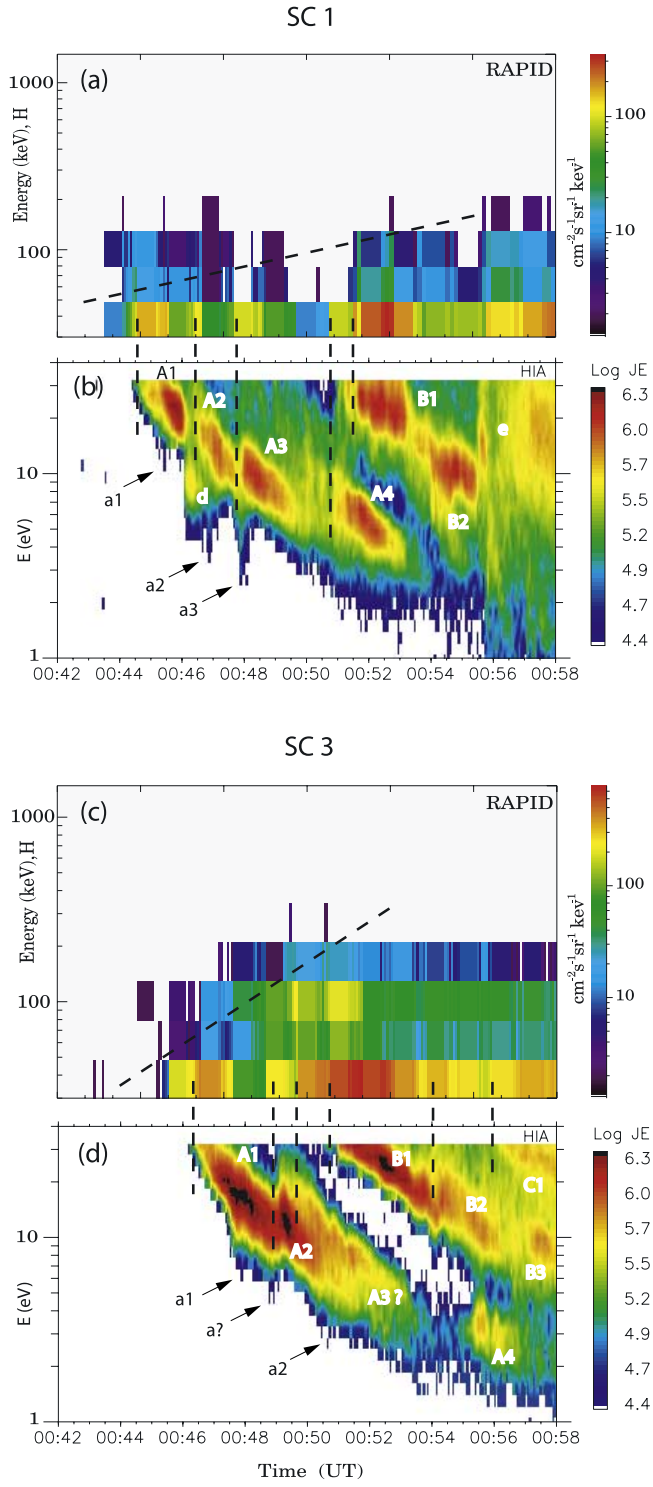

Figure 7. (a, c) RAPID and (b, d) CIS data covering together an energy range from 1 to 1500 keV. Data are omnidirectional with 4-s time resolution. Vertical lines show the connections between beamlets seen in the CIS and RAPID data. The beamlets are labeled for easier reference in the text. The slanted dashed lines indicate the increase in energy and/or energy flux of the second structures (B) compared to the first ones (A). The structures labeled "a1," etc., are associated with individual beamlets and are part of a steep energy dispersion that goes to high energies (>50 keV).

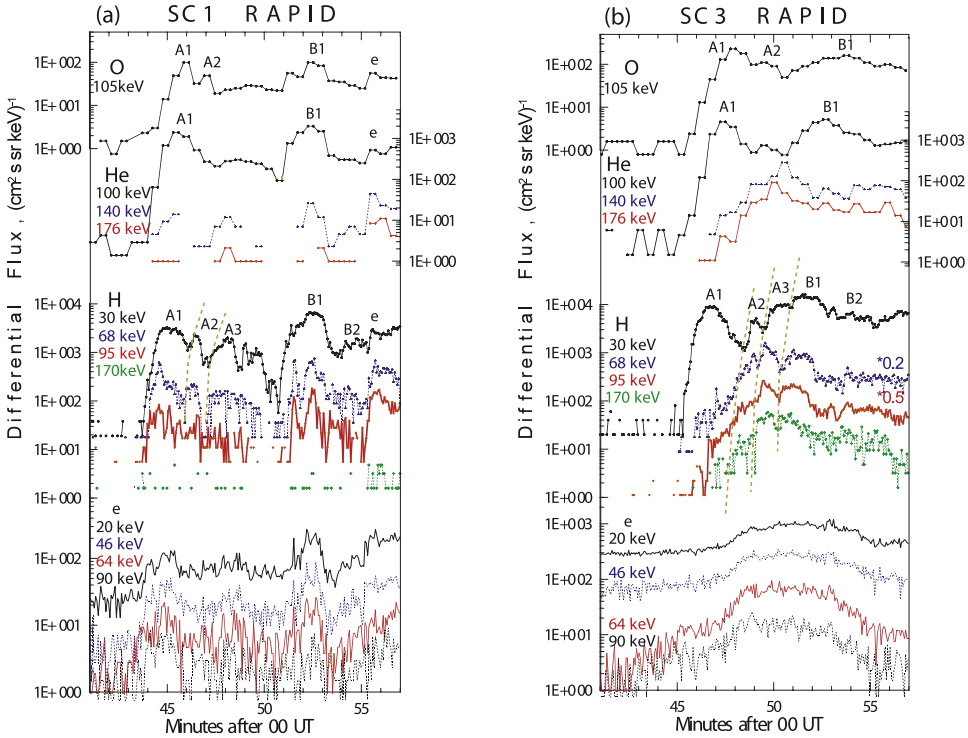

Figure 8. Differential flux versus time plots of O^+, He^+, H^+, and electrons from RAPID for (a) SC 1 and (b) SC 3. Individual beamlets are labeled. As examples several dashed brown lines illustrate the connection of similar features across different energy channels.

[25] The lower energy threshold of the beamlets extends below the energy associated with the peak energy fluxes (red and yellow in Figures 7b and 7d). Arrows (labeled a1, a2, a3, and a?) point to extended, nearly vertical ion structures below individual beamlets. In section 3.3.3 we show that these structures are part of the beamlets and that they are signatures of impulsive acceleration processes in the magnetotail.

[26] In comparing the energy ranges of the first structure (A) with the second structure (B) of SC 3 (Figure 7c), one finds that the energies and the energy fluxes (at a given energy) of the second structure are higher by several tens of keV (also indicated by the slanted dashed line). An energy difference is also present between structures A and B of SC 1 although not as pronounced. In addition, there is an energy difference of ~10 keV at the peak energy flux of B1 compared to A1 (SC 3, Figure 7d).

[27] We conclude that an acceleration mechanism acted on individual ion beamlets, was effective for different ion species, and led to a very broad energy range from a few keV up to at least 170 keV (bearing in mind the coarse resolution of each energy channel at high energies). The significance of the energy difference between structures A and B is discussed in section 3.4.

3.3.2. Angular Properties of Beamlets

[28] Figure 9 shows pitch angle-time spectrograms for SC 1 and SC 3 and velocity space distribution functions for SC 1. The energy range for the different pitch angle-time spectrograms was chosen such that different beamlets are represented. (The ion structures labeled "d" and "e" are discussed in section 3.5.)

[29] Pitch angle dispersion is present in all beamlets (see, e.g., A1 of both SC 1 and SC 3) except for B1 of SC 1. We interpret the upgoing ions (pitch angle <90°) of the beamlets as simply downgoing ions (pitch angle >90°) mirrored at lower altitude in the converging Earth's magnetic field. This can also be seen in the 2-D velocity space distribution functions from HIA (Figures 9i–9k). The first distribution function shows enhanced velocity space density of downgoing ions in the lower half-circle (arrow in Figure 9i). One integration period later (12 s) the distribution is almost isotropic (Figure 9j). The decrease in velocity space density at the top ($v_\perp \sim 0$) of this distribution is not interpreted as the loss cone because this feature disappears in later distribution functions and similar features appear at other locations in these distribution functions. Hence the feature in Figure 9i is probably a coincidence. Another integration period later, enhanced density is mostly present in the upper half, which corresponds to upgoing ions (arrow in Figure 9k). (The density enhancement of the parallel velocity at $v_{||} = -1000$ km in the lower half is due to a different ion structure, "d".) We also note that the circle of maximum velocity space density in Figure 9j is shifted toward positive velocities; that is, tailward moving particles moved faster compared to simultaneously arriving earthward moving particles. This behavior has been reported before [e.g., *Forbes et al.*, 1981; *Takahashi and Hones*, 1988]. From these distribution functions it is not possible to conclude whether the ion population was beamlike or isotropic at the source. For example, a beamlike distribution with a pitch angle of ~13° at 20 R_E (assuming a magnetic field of 20 nT) becomes isotropic at 4 R_E (400 nT) because of conservation of the magnetic moment.

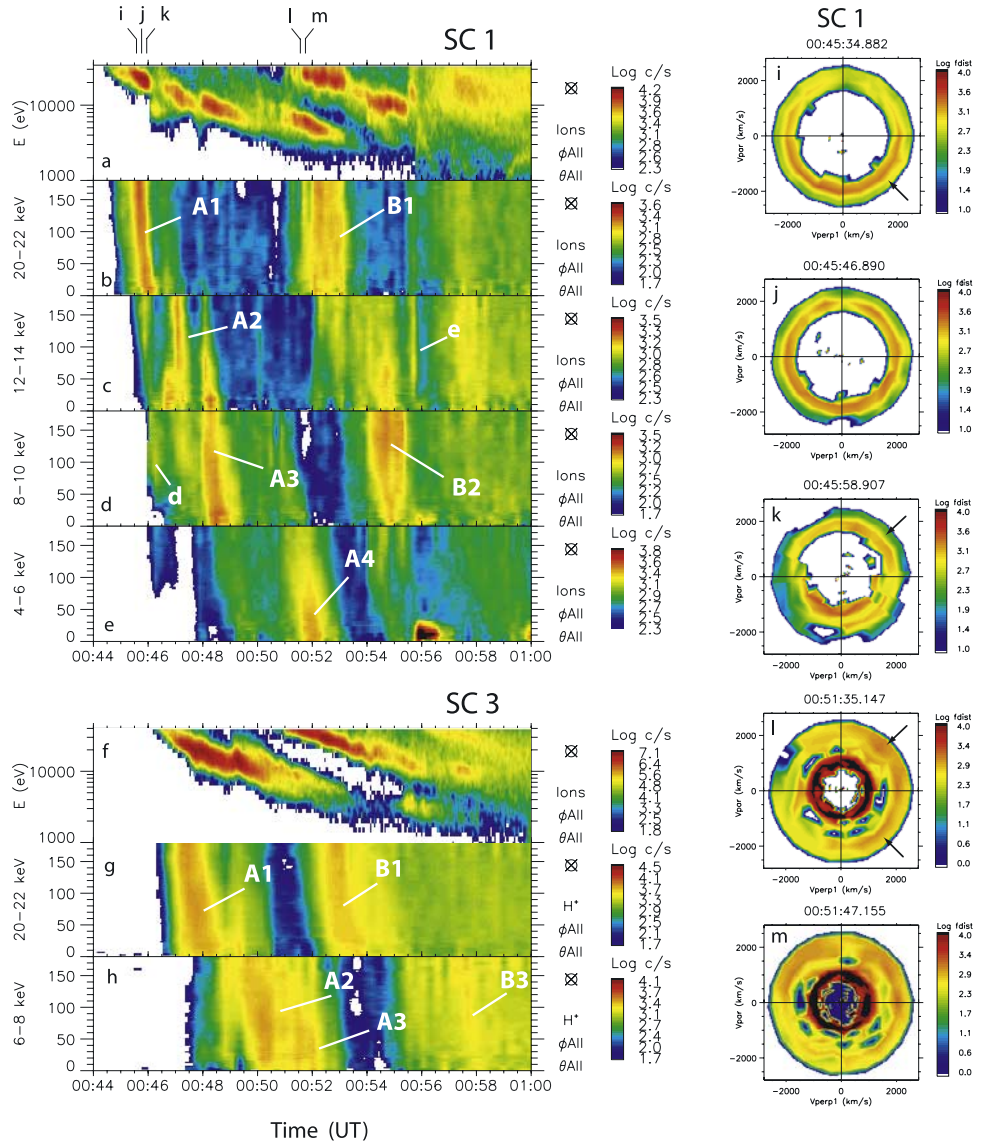

Figure 9. Pitch angle-time spectrograms for (a–e) SC 1 and (f–h) SC 3. Individual beamlets are labeled. (i–m) Velocity space distribution functions (averaged on board over 12 s) for SC 1. The times of these distribution functions are also indicated above Figure 9a.

[30] Figures 9l and 9m illustrate the change in the distribution functions during the crossing of beamlet B1 of SC 1. On entering B1 the distribution is such that positive velocities of $v_\perp$ show enhanced phase space density (Figures 9l and 9m, arrows). After that, the distribution becomes more isotropic. This signature could be interpreted as a finite ion gyroradius effect of plasma sheet ions at a spatial boundary. We note, however, that such a signature was not found for the other beamlets. In addition, this beamlet shows neither pitch angle dispersion (Figure 9b) nor energy dispersion for different species (Figure 8a) in contrast to all other beamlets. At present, it is not understood what makes this beamlet different from the other ones.

[31] Furthermore, we note that some beamlets have higher fluxes in a particular direction. For example, the dominant ion flow direction of A3 and A4 of SC 1 is up, with somewhat more equal contributions of downgoing ions for A3 (Figures 9d and 9e). This variation could be interpreted as a temporal signature. If we assume that A1–A4 were injected simultaneously for a short period, SC 1 may have encountered different parts of these ion beams because of their different velocities and because of the motion of SC 1 across different L shells. That is, when SC 1 reached the field line on which beamlet A4 was traveling, most of the downgoing ions had already passed, and only reflecting particles were encountered. In the case of A3, both downgoing and upgoing ions were still more equally present. In section 4.2 we refer to this signature as "trailing effect." On the other hand, one might explain this signature as a spatial effect, namely, that downgoing and upgoing ions $\mathbf{E} \times \mathbf{B}$ drift and thus return to different locations, which could lead to a missing component in the spacecraft measurements. Clearly, the single-spacecraft measurement (SC 1) still carries its spatiotemporal ambiguity, and thus no firm conclusion can be drawn from this. We also note that A2 of SC 1 shows a surprising transition from

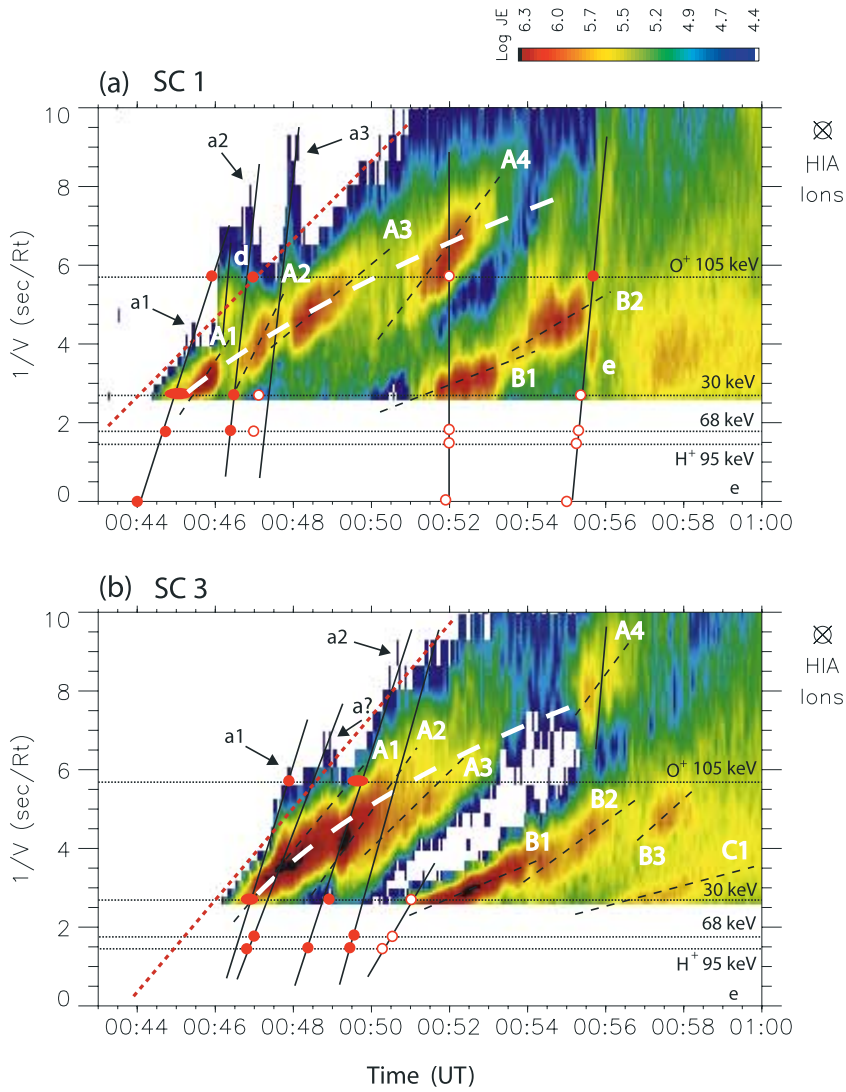

Figure 10. Inverse velocity versus time spectrograms for (a) SC 1 and (b) SC 3 (HIA, 4 s, omnidirectional). RAPID data in the form of red solid and open circles placed on horizontal dotted lines is included. See text for more description. The three energy dispersion slopes (dashed white line, dashed black line, and solid black line) associated with the dispersed ion structures and the beamlets are illustrated. The labels a1, a2, etc., point to ion structures that are associated with transient acceleration processes. The dashed red line indicates the systematic decrease of the low-energy cutoff of the ion PSBL.

first upgoing ions and then downgoing ones. This could indicate that this beamlet is actually fragmented into two.

3.3.3. Dispersion Slopes of Beamlets

[32] One of the most intriguing properties of the beamlets is the presence of three different energy dispersions. These dispersions are best investigated by displaying the data as inverse velocity versus time spectrograms (Figure 10). Each of the three dispersions discussed here is marked by a different line style. All lines were fitted visually. The dashed red line marks the systematic decrease of the lower energy cutoff (LEC) of PS ions versus time and latitude (in the spacecraft frame). This LEC could be caused by the $\mathbf{E} \times \mathbf{B}$ drift of the outer boundary particles ("convection filter") that map into the distant X line.

[33] The dashed white lines indicate the first energy dispersion, which is due to the decrease in mean energy of each beamlet. It appears as if the beamlets are grouped to form larger structures. This dispersion does not follow the LEC. Instead, the lower the mean beamlet energy (larger v^{-1} value), the farther away from the LEC the beamlet is located. This is the only energy dispersion that has been reported in the literature in association with the entire continuously traced ion structures. Because of the presence of beamlets in this event we find that each beamlet shows an additional dispersion (dashed black lines in Figure 10) which is steeper than the overall dispersion (dashed white line). The slopes of this second dispersion vary slightly for different beamlets, bearing in mind that there is some uncertainty in fitting the slope lines. The slopes of the beamlets of structure B (SC 1 and SC 3), however, are generally shallower compared to those of the beamlets of structure A. Furthermore, we note that when

extending the dashed black lines, they do not meet at the same time (same point on the $v^{-1} = 0$ line). Likewise, when plotted as inverse velocity versus ILAT (not shown), the dashed black lines do not meet at the same ILAT.

[34] To discuss the third energy dispersion, we included RAPID data in the form of red circles (solid and open) in Figure 10. Horizontal dotted lines indicate the v^{-1} values that hydrogen and oxygen ions for given energies would have in this plot. Electrons are represented by the line $v^{-1} = 0$. The circles were inferred from Figure 8. Solid (open) circles refer to peak values (beginning of steep slopes) of identifiable features in Figure 8. We only included features as circles if we could identify them in at least two energy channels of hydrogen. A few examples of features that appear to be related are connected by dashed brown lines in Figure 8. In Figure 10, solid black lines are drawn through the circles (RAPID data points) that are likely to be related. The third line from the left for SC 1 is slightly displaced, allowing for the fact that the open circles indicate the beginning and not the maximum of the feature. It is apparent that the solid black lines have different slopes than the dashed black and white lines. Thus these solid black lines represent the third energy dispersion. As already mentioned in section 3.3.2, B1 of SC 1 shows no energy dispersion across different energy channels and different species, which can again be seen in Figure 10a as a vertical black line at 0052 UT. A special discussion of the solid black line passing through A4 (Figure 10b) is given in section 3.5 together with a discussion of the structure "e" (Figure 10a).

[35] Although the solid black lines were drawn on the basis of RAPID data, there are features in the CIS data (a1, a2, a3, and a? in Figure 10) at lower energy, which line up with the solid lines. These features are the same ones that we pointed out in Figure 7. This suggests that the very high energies (>50 keV) are related to the lower energies (<10 keV) through a common acceleration mechanism acting over a very broad energy range. Importantly, each of these dispersion slopes (solid black line) appears to be associated with a beamlet. The first dispersion slope from the left is associated with A1 and so on for both spacecraft. In Figure 10b the second solid black line from the left goes through the feature that was labeled "a?." We used this label to indicate that an intermediate beamlet is not clearly visible but imaginable so that A1 of SC 3 could, in fact, consist of two beamlets.

[36] We have reason to believe that this third energy dispersion, which extends over a very large energy range, is of temporal nature for the following reasons. First, it is much steeper than the presumed spatial dispersion of the LEC (dashed red line) and also much steeper than the first and second energy dispersions discussed above, thus indicating that it is of different origin. Second, the energy range and the steepness of this third energy dispersion are similar to those of the transient ion injection "e" (Figure 10a), suggesting that both are generated by the same impulsive acceleration process (see also section 3.5). On the basis of this temporal interpretation we can determine the acceleration location of this third dispersion. Using the inverse of the line slope as an indicator for the travel distance, we obtain 7–18 R_E (SC 1) and 16–23 R_E (SC 3) for the travel distances. Together with the location of the spacecraft of

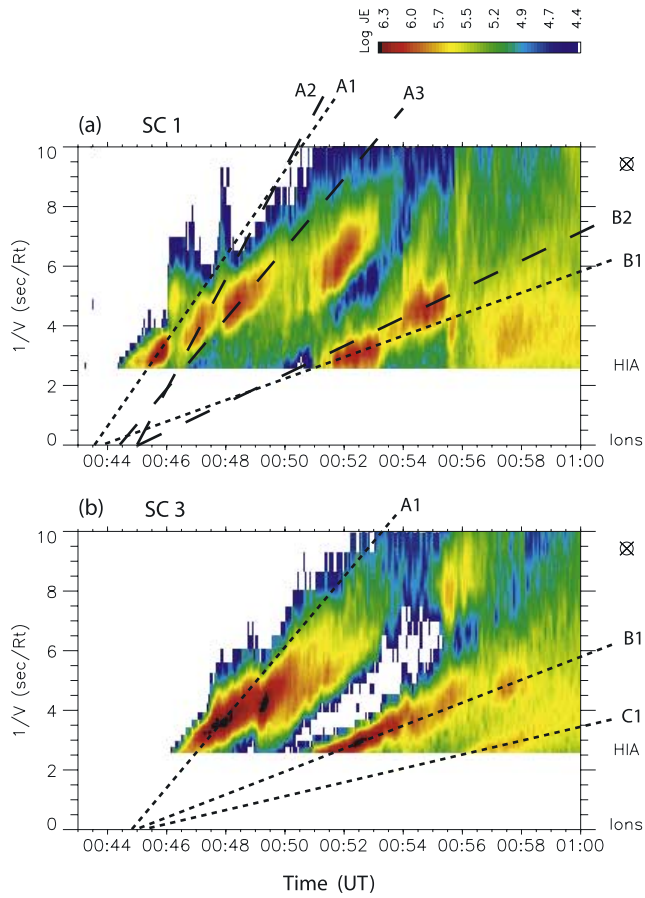

Figure 11. Inverse velocity versus time spectrograms for (a) SC 1 and (b) SC 3 (HIA, 4 s, omnidirectional), illustrating the bouncing properties of beamlets.

4.5 R_E, this yields acceleration regions from 11–22 R_E and 20–27 R_E, respectively, in the magnetotail. The different source regions for this third dispersion recorded by the two spacecraft make it again plausible that the ions underwent different spatiotemporal histories, which resulted in different slopes and different beamlet numbers.

[37] We interpret these observations as follows: (1) The dashed white line cannot represent the dispersion of a continuously traced structure because it is shallower than the LEC which would otherwise imply a travel distance of ions that is farther than the source region of the LEC. (2) It is possible, using the observation of the second dispersion slope (dashed black lines), that the beamlets were injected from an extended source, covering many L shells such that lower energetic beamlets were injected on field lines with smaller L values or, equivalently, closer to Earth if injected in the equatorial plane similar to the scenario reported by *Takahashi and Hones* [1988]; this scenario is IDIS. (3) In addition to the IDIS scenario we propose a scenario in which the beamlets were created during the flight for which some evidence exists in the form of the third energy dispersion (solid black lines); a more detailed discussion on the two scenarios is given in section 4. (4) The generally shallower slopes of the B beamlets compared to the A beamlets can be explained by assuming that the former beamlets are echoes of the latter ones as shown in section

Table 1. Ratios of Various Beamlet Dispersion Slopes in Comparison With Idealized Ratios of Bouncing Ions

Slope Ratios	Ideal Ratio	Measured Ratio
	SC 1	
A1:B1	1:3	1:(3.8 ± 0.7)
(A2 or A3):B2	1:3	1:(3.2 ± 1.0)
	SC 3	
A1:B1:C1	1:3:5	1:(3.1 ± 0.7):(4.9 ± 1.0)

3.4. (5) The similarity of the second dispersion slopes (dashed black lines) of individual beamlets with the slope of the LEC suggests an ion source region at great distances (>30 R_E) and a similar generation mechanism of LEC and ion structures.

3.4. Bouncing Beamlets

[38] In section 3.3 we showed that beamlets were grouped into larger structures, and we identified some of their properties. Another important issue to address is the origin of these ion structures. In this section we show evidence that the second (B) and third (C) structures are echoes of the first (A). The origin of A will be discussed in section 4. The term "echo" describing bouncing ion beamlets was first introduced by *Ashour-Abdalla et al.* [1992], who predicted echo beamlets in the PSBL.

[39] Again, we use inverse velocity versus time spectrograms but this time focus on a few beamlets (Figure 11). We have visually fitted straight lines through some beamlets of the structures A, B, and C. Bearing in mind the uncertainty in fitting straight lines through the beamlets, the lines through A1 and B1 of SC 1 (small dashed lines) nearly intercept each other at the line $v^{-1} = 0$. The same can be said for the large dashed lines through A2 (or maybe A3) and B2. These common intercepts suggest a relationship between the corresponding beamlets, namely that depending on the type (VDIS/IDIS or TDIS), the corresponding beamlets were either ejected at the same location, the same time, or both. The uncertainty in fitting the lines somewhat weakens the interpretation of bouncing ions. However, the observations of SC 3 have the advantage that a third dispersed structure (C), although faint, is available. In this case, the fitted straight lines of the three beamlets A1, B1, and C1 approximately intercept at the same point on the $v^{-1} = 0$ line. In addition, the dispersion slopes of A1, B1, and C1 get progressively shallower, which implies an increasing travel distance, and the time delay for a given energy from A1 to B1 is roughly equal to the time delay from B1 to C1. The common intercepts, the increasing travel distance, and the equal spacing between successive structures suggest that the beamlets of B and C are the first and second echoes, respectively, of the beamlets of A.

[40] Two possibilities exist with regard to bouncing ions ejected bidirectionally in the distant tail. The first possibility is that ions travel toward the lower-altitude observation site (Cluster spacecraft) and are then reflected below the spacecraft in the strong converging Earth magnetic field, which happens in both hemispheres. The ions then cross the current sheet and travel toward the opposite ionosphere where the particles are again reflected. Alternatively, the ions do not cross the current sheet but instead are scattered back in the current sheet in the direction from which the particles came. These two possibilities yield a travel distance ratio of 1:3:5 associated with one ion source and two echoes, assuming that the spacecraft is much closer to the low-latitude reflection location than to the injection location. In Table 1 we have calculated the ratios of the slopes (dashed lines in Figure 11), which are functions of the travel distances for both VDIS and TDIS. We have included errors derived from the slope uncertainties (determined by graphical means). These ratios, together with the signatures mentioned in the previous paragraph, suggest that the ion structures B and C are indeed echoes as opposed to independent ion injections. The fact that the ratios do not exactly fit the model does not substantially weaken the argument for echoes. Additional acceleration in the consecutive neutral sheet crossings, shortening of the magnetic field lines due to convection, and a spacecraft location away from the reflection point will change this ratio. We also note here that we had to use the slope values of corresponding beamlets to obtain travel distance ratios that are close to the ratios of bouncing ions. The slope values of the entire structures (dashed white lines in Figure 10) do not yield ratios that indicate bouncing ion structures.

[41] Finally, the number of echo beamlets in a large-scale structure is reduced with respect to the preceding large-scale structure. This might indicate that more and more beamlets become diffuse (thermalized) and disappear while crossing the neutral sheet repeatedly until all beamlets are thermalized and form the CPS. Moreover, it appears that the echo beamlet (B1) on SC 3 gained about 10 keV energy (compare energies at peak energy flux for A1 and B1 in Figure 7d). This gain could be due to additional neutral sheet acceleration during additional neutral sheet crossings.

3.5. Transient Ion Injections

[42] In addition to the large-scale dispersed ion structures A, B, and C and their associated beamlets, two transient, narrow dispersed ion structures (labeled "d" and "e" in Figures 3, 7, 9, and 10) were recorded at ~0046 and ~0055:30 UT by SC 1 (not observed by SC 3 and SC 4). They lasted for only ~15 s in the spacecraft frame as opposed to ~1 min for the large-scale structures. Structure "d" is only seen with pitch angles >50°, indicating the temporal character of this structure (Figure 9d). Because it is a very narrow structure, the spacecraft probably missed the reflecting particles (lower pitch angles). On the other hand, structure "e" covers nearly all pitch angles (Figure 9c).

[43] The structure "e" (not "d") is also seen in the RAPID data (Figures 8 and 10) for different ion species, covering a very large energy range from 2 to 140 keV. Using the inverse of the line slope (Figure 10a) as an indicator for the travel distance, we obtain ~6 R_E for the travel distance of "e." Together with the location of SC 1 (4.5 R_E), this yields an injection location of ~11 R_E in the tail. The structure "d" shows the same slope as "e" so that the same travel distance is obtained. We emphasize that both structures were injected on field lines with very different L values inside the PSBL.

[44] In section 3.3 we described in detail the three different energy dispersions associated with beamlets. It

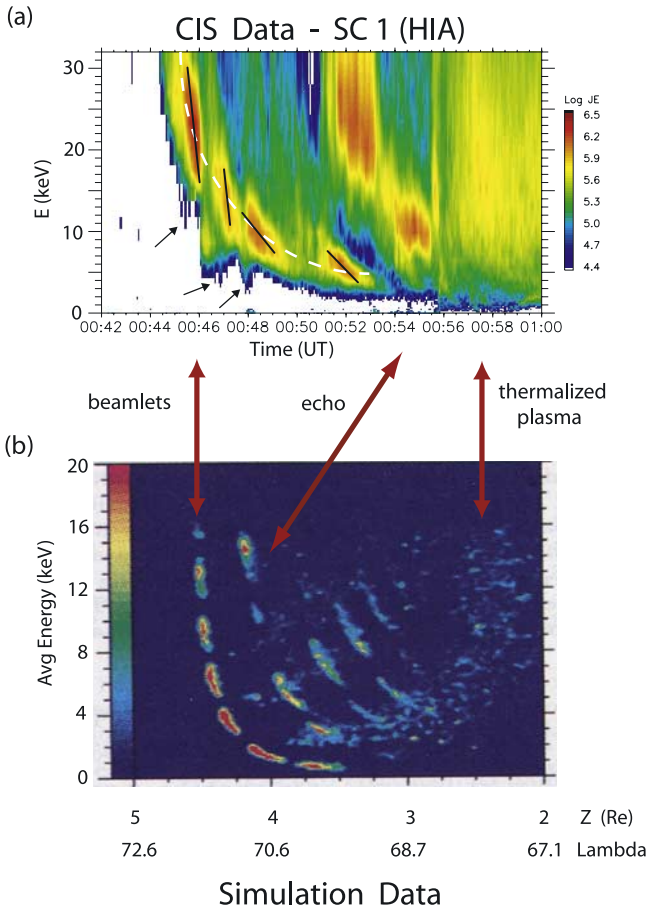

Figure 12. Comparison of (a) CIS data and (b) simulation data (Figure 2b of *Ashour-Abdalla et al.* [1992]).

turned out that one energy dispersion had very similar slopes compared to the slopes of "d" and "e." This suggests that the two structures and this particular beamlet dispersion might have resulted from the same temporal acceleration processes at similar distances, acting over a range of L shells, possibly the entire PSBL.

[45] We also note here that beamlet A4 of SC 3 (Figure 10b) is split into two structures. The solid black line passing through A4 is the same as for structure "e" (Figure 10a); time and slope are identical. It can be seen that the dispersion of structure "e" nearly coincides temporally with the second part of beamlet A4. It is thus suggestive that the splitting is related to or caused by the same acceleration process that generated structure "e." However, we cannot rule out that this example is a coincidence. The idea of splitting ion structures by impulsive acceleration processes is the basis of one possible scenario (section 4.2) that can explain the beamlet structures.

4. Interpretation of Observations

[46] We have presented observations of multiple energy-dispersed ion structures in the PSBL. The multiplicity was interpreted as echoes. The most intriguing feature, however, was the clear signature of beamlets. In this section we give two scenarios to explain the origin of the beamlet structure. One of them relies on a simulation described in the literature, whereas the other one incorporates new ideas and is less quantitative.

4.1. First Scenario

[47] The 14 February 2001 observations can be compared with results from a particle simulation by *Ashour-Abdalla et al.* [1992]. Their simulation followed ions as they convected from the plasma mantle into the magnetotail current sheet where the ions find themselves in alternating regions of enhanced trapping and ejection. The accelerated and ejected ions follow Speiser orbits [*Speiser*, 1967], form the PSBL, and give the dispersed ion structures their peculiar beamlet structure. The amount of acceleration at a particular position along the current sheet is also a function of the magnetic field component perpendicular to the current sheet at this position [*Zelenyi et al.*, 1990]. In the simulation a static tail magnetic field with monotonically decreasing normal component in the negative x (GSE) direction and a neutral line at 100 R_E were used. In this configuration the simulated beamlets closer to the neutral line gained larger energies. This spatial dependency is called intrinsic dispersion [*Zelenyi et al.*, 1990]. It translates into the PSBL such that from the lobe-PSBL interface toward the CPS the ions have lesser energies. Figure 1c (section 1) shows a representation of the intrinsic dispersion model, without showing the beamlet/gap formation (see instead *Ashour-Abdalla et al.* [1993] for a more complete description).

[48] The results of this simulation (virtual measurements in the PSBL at X = -7 R_E) are shown in Figure 12 in comparison to CIS data from the 14 February 2001 event. For better comparison, the CIS data are displayed with a linear energy scale. The following similarities can be identified: (1) Several well-separated beamlets with different energies exist. (2) The beamlets appear to be embedded into a larger structure. (3) Several echo beamlets of the original beamlets exist at lower L values (see also Figure 11b). (4) In the simulation the echo beamlets have higher energies (+2 keV) compared to the initial beamlets, and although this is not apparent for the ion structure recorded by SC 1, it is the case for SC 3 (Figure 7d) where the gain is about 10 keV for the peak energy fluxes. (5) Initial and echo beamlets can occur on the same field line (same L value). (6) The number of echo beamlets inside the large-scale structure is reduced compared to the number inside the initial large-scale structure. (7) Echo beamlets are progressively more diffuse, leading eventually to the thermalized plasma of the CPS (see also Figure 10b).

[49] Some features in the observations, however, do not match the simulation or were not addressed by it:

[50] 1. In the CIS data the energy ranges of adjacent beamlets overlap, whereas in the simulation they do not.

[51] 2. Individual beamlets (CIS data) show varying dispersion slopes (black lines in Figure 12), but in all cases these slopes are steeper compared to the dispersion associated with the large-scale structure (dashed white line). This can also be seen well in Figure 10, where we also show that these beamlet dispersion slopes did intercept the $v^{-1} = 0$ line at different times and different ILAT, which is the signature of IDIS. We note that no inverse velocity versus time plot for the simulation results is available for further comparison.

[52] 3. Simulation beamlets do not show the ion structures (black arrows in Figure 12) that we labeled a1, a2, and

a3 in Figure 7. These structures were part of a third steep energy dispersion associated with individual beamlets as observed by CIS and RAPID. This dispersion was caused by a transient acceleration process that covered a broad range of energies (a few keV to >100 keV) and acted on different ion species.

[53] 4. In addition to the energy gain of the peak energy fluxes mentioned in item 4 (above), the first echo beamlets gained energies of more than 30 keV up to 170 keV (Figures 7 and 8). This gain is too large to be caused by neutral sheet acceleration alone.

[54] 5. Observed beamlets did not follow the LEC (see also Figure 10). This boundary is not shown in the simulation.

[55] With regard to the model assumptions we make the following remarks. The acceleration mechanism in the simulation is neutral sheet acceleration. This mechanism depends on the presence of reconnection which generates/requires a dawn-dusk electric field. This field is present throughout the neutral sheet and is expected to cause the particle acceleration. The energy gained depends on the strength of the dawn-dusk electric field (or equivalently on the dawn-dusk potential drop). In the simulation a homogenous dawn-dusk electric field of 0.1 mV m^{-1} was used. The dawn-dusk potential drop typically can reach values up to 80 kV [see *Möbius et al.*, 1980, and references therein] during disturbed periods. This puts a limit on the energy that can be gained by the neutral sheet acceleration mechanism. In the CIS observation the most energetic particles at the peak fluxes had energies up to the energy limit of the instrument (40 keV), which is within the range of neutral sheet acceleration. However, RAPID data show low fluxes of particles that were associated with the CIS beamlets with energies above 100 keV. It is arguable whether this can be generated with neutral sheet acceleration alone. Furthermore, we gave evidence that the highest energies were associated with an additional transient acceleration process at 11–27 R_E, which is closer than the location of the ion source region in both the simulation and the observation (>30 R_E).

[56] Furthermore, in the simulation the normal component of the tail magnetic field monotonically falls off with distance up to the neutral line at 100 R_E. In a static dipolar field this is indeed the case, but it is arguable how this translates to a dynamic magnetotail where the magnetic field is fluctuating. We note, however, that although Kp = 4− and AE = 326 nT (averaged), the magnetosphere was likely to be in the recovery phase, which favors a far-tail neutral line and a more stable tail magnetic field. We also showed evidence for a retreating neutral line and a retreating ion source which was not simulated. Hence additional simulations to determine whether the PSBL retains its beamlet structure under these conditions will be required.

[57] In summary, both beamlets and gaps are spatial structures in the simulation. We showed some evidence that the beamlets could indeed have been injected from different sources along the neutral sheet. However, the simulation did not include any temporal effects for which we also presented evidence. We showed transient acceleration processes which led to a third steep energy dispersion associated with individual beamlets. This acceleration must have occurred at distances closer than the ion source regions. It is not clear how to incorporate this temporal aspect into the quasi-static picture of the simulation. In addition, the broad energy range of the temporal acceleration is not covered by the simulation. Currently, there is no alternative model in the literature supported by a numerical simulation that generates the beamlet structure as was observed in the 14 February 2001 event. Because of its current limitation in explaining all observations and because of some of its debatable assumptions, alternative models need to be considered.

4.2. Second Scenario

[58] A radically different explanation for the beamlet structure is to hypothesize its formation after ejection, or in other words, during the flight. The four beamlets of structure A (SC 1) appear to be embedded in a larger-scale structure so that it is possible to imagine that they had been generated by one source as opposed to several sources along the neutral sheet as proposed in section 4.1. Indeed, if we remove the gaps, a continuously traced "mother" structure (which is usually reported in the literature) is created, in particular for SC 1, except that slopes of individual beamlets are steeper than the overall slope of the "mother" structure (see next paragraph for an explanation). The overlapping energy ranges of adjacent beamlets, which were in contrast to the simulation results of section 4.1, can thus be easily explained here.

[59] In this second scenario we suggest that the beam particles selectively undergo additional acceleration away from the initial injection location in specific places with a quasi-period of 1–3 min. This acceleration might then separate beam particles into beamlets and could steepen the dispersion slope of individual beamlets as observed. The apparent temporal coincidence of the second beamlet of structure A of SC 3 and SC 4 (section 3.2) supports this view. The splitting of A4 (SC 3) at the same time when the transient acceleration occurred that led to the structure "e" could be a direct observation of this process, although we did not rule out that this was coincidental (section 3.5).

[60] The strongest evidence for a recurrent impulsive acceleration process causing the beamlet structure is the observed temporal steep energy dispersion at the beginning of each beamlet. This additional energy dispersion exceeded the energy range of the main fluxes of the "mother" structure and thus indicated an additional acceleration process. We estimated the radial distance of the acceleration region to be 11–27 R_E. This distance is closer than the distance where the "mother" dispersed ion structures were most likely generated (>30 R_E) and thus supports the view that the beamlet structure was created after injection.

[61] Given the possibility that the beamlet structures were created during the flight, one is still left with the problem of how the initially unstructured "mother" ion structures covering the energy range from 2 to 40 keV were generated in the first place. Reconnection or neutral sheet acceleration are two possible candidates. The "trailing effect" (section 3.3.2) observed in structure A of SC 1 and the retreating ion source (section 3.2) are compatible with a temporal ion structure. Alternatively, one could imagine that ions were quasi-continuously ejected similarly to the VDIS model. We also remind the reader that the similarity of the slopes of the first and second energy dispersions (dashed white and black lines in Figure 10) with the slope of the LEC suggests a similar generation mechanism of these signatures.

[62] With regard to the recurrent impulsive acceleration mechanism at 11–27 R_E we make the following remarks:

[63] 1. This acceleration mechanism acted on many L shells of the PSBL and generated a broad range of energies (a few keV to at least 170 keV).

[64] 2. Since the beamlet structures at SC 1 and SC 3 (azimuthally separated by only 100 km) were very different, this would imply that no exact temporal synchronization of beamlet formation at different locations in the PS existed. We also showed that the acceleration regions associated with the two beamlet structures recorded by SC 1 and SC 3 were different: 11–22 and 20–27 R_E radial distance, respectively. This suggests that at least two acceleration regions existed, which were localized in both the x and y (GSE) directions.

[65] 3. The impulsive accelerations occurred during the recovery phase as indicated by some magnetospheric signatures. We rule out that this impulsive acceleration was associated with reconnection at a retreating far-tail neutral line during the recovery phase.

[66] 4. The beamlet occurrences, or equivalently the occurrence of the impulsive acceleration processes, varied between 1 and 3 min. This timescale can be found for other magnetospheric phenomena (see the review by *Sergeev et al.* [1996]): The formation of successive poleward arcs occurs every 1–3 min, proton injections at geosynchronous orbit have an average repetition time of 2.6 min, and the repetition time of bursts in a bursty bulk flow event is 1–3 min. These phenomena have been linked to impulsive reconnection.

[67] In summary, the hypothesized beamlet generation mechanism described in this section assumes two different regions that were responsible for the generation of the beamlets: one farther out in the tail (>30 R_E) that created the "mother" ion structure and one closer in (<30 R_E) that created the beamlet structure. Current substorm models cannot explain this scenario. Computer simulations are required to quantitatively validate the ideas that have been described here very qualitatively.

5. Summary and Further Discussion

[68] In this study we identified new properties of multiple energy-dispersed ion structures using multipoint CIS and RAPID measurements, covering an energy range between a few eV and 1500 keV, during a PSBL crossing (0.1 MLT, 4.5 R_E) on 14 February 2001. The availability of low (<40 keV)- and high (>40 keV)-energy ion data revealed a great complexity. The PSBL was highly structured, showing several large-scale dispersed ion structures, which were substructured into several (up to four per large-scale structure) beamlets. These dispersed ion structures and their beamlets had the following characteristics. (1) Beamlets existed for different ion species: H^+, O^+, and He^+. (2) Three different energy dispersion slopes were associated with the ion structures. (3) The energy dispersion of the large-scale structures covered energies from 2 to >40 keV. (4) The dispersion slopes following the peak flux line of individual beamlets were steeper than the overall energy dispersion slope of the larger-scale dispersed ion structure. (5) The origin of these two dispersions, described in characteristics 3 and 4, could not be conclusively established. (6) A third energy dispersion occurred at the beginning of each beamlet and covered an energy range from a few keV to >100 keV; this dispersion was associated with recurrent impulsive acceleration processes at 11–27 R_E radial distance with a quasiperiodicity of 1–3 min. (7) Most beamlets showed pitch angle dispersion. (8) Individual beamlets bounced and returned up to two times to the spacecraft location. (9) Bouncing beamlets acquired higher energies compared to their original beamlets. (10) After multiple bounces the beamlets became the thermalized, isotropic plasma of the CPS. (11) The beamlet structures varied greatly between different spacecraft that were azimuthally separated by only 100 km. (12) The dispersed ion structures were magnetically connected to the poleward arc of the double oval.

[69] We put the Cluster observations in the frameworks of both the *Ashour-Abdalla et al.* [1992] model and local recurrent impulsive acceleration at radial distances of 11–27 R_E. The main difference was whether the beamlet structure was already created at the source or later during the flight. The two scenarios are incomplete insofar as the first scenario does not account for all observations, and the second scenario, although incorporating many observational features, is not supported by theoretical work or computer simulations. The interpretation of the 14 February 2001 event was complicated by the fact that the PSBL was crossed from the southern lobe toward the equatorial plane, which is in the same direction as the presumed $\mathbf{E} \times \mathbf{B}$ drift motion of the ambient plasma. This means that the observed decline in ion energy of each dispersive ion structure (large-scale structures and beamlets) is both a decline with decreasing latitude, as would be expected with VDIS and IDIS, and a decline over time, as would be expected with TDIS. In spite of this ambiguity, we showed evidence for temporal acceleration processes that played at least one role (possibly the generation of the beamlet structure) in the complicated spatiotemporal history of particle acceleration in this event. We also identified many new properties of beamlets which will be useful for future theoretical and simulation work on plasma acceleration processes and beamlet structures in the magnetotail.

[70] The most distinctive features in the Cluster observations were the well-separated beamlets in the large-scale dispersed ion structures. Previous reports on beamlets (*Takahashi and Hones* [1988] (they did not use this term) and *Bosqued et al.* [1993]) were not able to resolve individual features of the beamlets. *Bosqued et al.* [1993] made observations at low altitude (<2000 km), whereas *Takahashi and Hones* [1988] made observations in the tail PSBL at 7–13 R_E. Both studies interpreted their observations in the framework of intrinsic dispersion. In a more recent study, *Sergeev et al.* [2000], reporting TDIS that were magnetically conjugate to the auroral bulge, suggested the possibility that one of the ion injections showed two smaller-scale structures which they called injectionlets. However, these injectionlets were not further discussed.

[71] We reported for the first time bouncing beamlets in the tail PSBL. So far, bouncing ion clusters have been reported in the auroral zone [*Bosqued et al.*, 1993; *Hirahara et al.*, 1996], the CPS [*Quinn and McIlwain*, 1979; *Sauvaud et al.*, 1999; *Kazama and Mukai*, 2003], and the dayside magnetosphere [*Quinn and McIlwain*, 1979]. An interesting observation for the 14 February 2001 event was that some

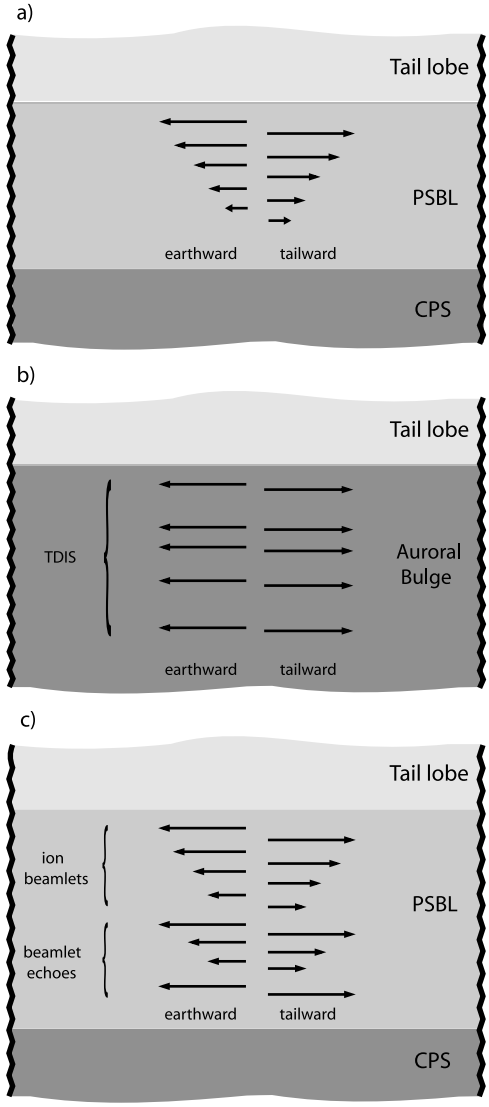

Figure 13. Schematics showing different ion structures in the PSBL and on auroral bulge field lines. (a) Adapted from Figure 16 of *Takahashi and Hones* [1988]. (b) Results from *Sauvaud et al.* [1999] and *Sergeev et al.* [2000] presented in a similar format as in Figure 13a. (c) The 14 February 2001 observations showing echoes and a more complicated layering of ion velocities.

echoes had higher energies compared to the initial ions, which can be attributed to additional acceleration in the current sheet during their second and third interactions with the current sheet. The bouncing beamlets in the PSBL also confirm that those field lines were closed.

[72] The upper energy limit of energy-dispersed ion structures, in particular for beamlets, has not been adequately reported in the literature. *Williams* [1981] showed energy dispersion for ion beams up to 2 MeV. Most studies that reported dispersed ion structures were, however, unable to comment on energies above 40 keV because the structures reached the upper energy limit of their particle detector. Thus it cannot be ruled out that higher energies were also associated with their events. It is this higher energy range (>40 keV) that facilitated the identification of the temporal acceleration processes, which could possibly have been responsible for the beamlet structure in our event. For the first time we showed that a beamlet structure was present for energies >100 keV. How this large range of energies, in particular for each beamlet inside the large-scale dispersive structure, was generated is not clear yet. Other studies [e.g., *Spjeldvik and Fritz*, 1981] have reported even higher particle energies (up to several hundred keV) for earthward directed fluxes of ions and electrons in the PSBL, but they were not associated with beamlets. In a more recent study, *Sergeev et al.* [2000] reported ion beams in the 3–14 keV energy range that were additionally associated with an impulsive acceleration mechanism up to hundreds of keV.

[73] A long-held view of ion beams in the PSBL is that the velocity profile of the layering of earthward and tailward streaming ions is decreasing from the lobe-PSBL interface toward the CPS [*Forbes et al.*, 1981; *Takahashi and Hones*, 1988] and that the tailward flowing ions are the reflected earthward flowing ions. In more recent studies new types of ion injections were reported. *Parks et al.* [1998] showed that the PSBL also consists of unidirectional earthward and tailward streaming ion beams. Recurrent injections of nonbouncing TDIS into the auroral bulge were presented by *Sauvaud et al.* [1999] and *Sergeev et al.* [2000]. These studies added new views on ion beams in the PSBL/CPS to the preexisting one. Our observation adds yet another view, namely, that of bounces (echoes) and more complicated ion layering. Our observations are illustrated in Figure 13c. For clarity, we drew the first echo beamlet below the last beamlet of the first large-scale ion structure, although the observation showed that these beamlets can occur on the same field line. The format of this figure was motivated by the well-known Figure 16 of *Takahashi and Hones* [1988]. For easier comparison, we added a simplified version of their figure and also presented the results of *Sauvaud et al.* [1999] and *Sergeev et al.* [2000] in the same format.

[74] **Acknowledgments.** We thank Harald Frey from the Space Science Laboratory, Berkeley, for providing data from IMAGE-FUV. We thank Ari Viljanen from the Finnish Meteorological Institute for the IMAGE ground magnetometer data. We thank K. Stasiewicz, M. Khotyaintsev, and Y. Khotyaintsev for providing the Orbit Visualization Tool (http://ovt.irfu.se). This work was carried out while A.K. held an ESA fellowship.

[75] Lou-Chuang Lee thanks O. Walter Lennartsson and Maha Ashour-Abdalla for their assistance in evaluating this paper.

References

Andrews, M. K., P. W. Daly, and E. Keppler (1981), Ion jetting at the plasma sheet boundary: Simultaneous observations of incident and reflected particles, *Geophys. Res. Lett.*, *8*, 987–990.

Ashour-Abdalla, M., L. M. Zelenyi, J. M. Bosqued, and R. A. Kovrazhkin (1992), Precipitation of fast ion beams from the plasma sheet boundary layer, *Geophys. Res. Lett.*, *19*, 617–620.

Ashour-Abdalla, M., J. P. Berchem, J. Büchner, and L. M. Zelenyi (1993), Shaping of the magnetotail from the mantle: Global and local structuring, *J. Geophys. Res.*, *98*, 5651–5676.

Boehm, M. D., D. M. Klumpar, E. Möbius, L. M. Kistler, J. P. McFadden, C. W. Carlson, and R. E. Ergun (1999), Fast auroral snapshot observations of bouncing ion distributions: Fieldline length measurements, *J. Geophys. Res.*, *104*, 2343–2356.

Bosqued, J. M., J. A. Sauvaud, D. Delcourt, and R. A. Kovrazhkin (1986), Precipitation of suprathermal ionospheric ions accelerated in the conjugate hemisphere, *J. Geophys. Res.*, *91*, 7006–7018.

Bosqued, J. M., M. Ashour-Abdalla, M. El Alaoui, V. Peroomian, L. M. Zelenyi, and C. P. Escoubet (1993), Dispersed ion structures at the poleward edge of the auroral oval: Low-altitude observations and numerical modeling, *J. Geophys. Res.*, *98*, 19,181–19,204.

Cowley, S. W. H. (1980), Plasma populations in a simple open magnetosphere, *Space Sci. Rev.*, *26*, 217–275.

Eastman, T. E., L. A. Frank, W. K. Peterson, and W. Lennartsson (1984), The plasma sheet boundary layer, *J. Geophys. Res.*, *89*, 1553–1572.

Elphinstone, R. D., et al. (1993), The auroral distribution and its mapping according to substorm phase, *J. Atmos. Terr. Phys.*, *55*, 1741–1762.

Elphinstone, R. D., et al. (1995), The double oval UV auroral distribution: 2. The most poleward arc system and the dynamics of the magnetotail, *J. Geophys. Res.*, *100*, 12,093–12,012.

Forbes, T., et al. (1981), Evidence for the tailward retreat of a magnetic neutral line in the magnetotail during substorm recovery, *Geophys. Res. Lett.*, *8*, 261–264.

Frank, L. A., K. L. Ackerson, and R. P. Lepping (1976), On hot tenuous plasmas, fireballs, and boundary layers in the Earth's magnetotail, *J. Geophys. Res.*, *81*, 5859–5881.

Hasegawa, A. (1987), Beam production at plasma boundaries by kinetic Alfvén waves, *J. Geophys. Res.*, *92*, 11,221–11,223.

Hirahara, M., T. Mukai, T. Nagai, N. Kaya, H. Hayakawa, and H. Fukunishi (1996), Two types of ion energy dispersions observed in the nightside auroral regions during geomagnetically disturbed periods, *J. Geophys. Res.*, *101*, 7749–7768.

Kan, J. R., and S.-I. Akasofu (1976), Energy source and mechanisms for accelerating the electrons and driving the field-aligned currents of the discrete auroral arc, *J. Geophys. Res.*, *81*, 5123–5130.

Kazama, Y., and T. Mukai (2003), Multiple energy-dispersed ion signatures in the near-Earth magnetotail: Geotail observation, *Geophys. Res. Lett.*, *30*(7), 1384, doi:10.1029/2002GL016637.

Lyons, L. R., and D. S. Evans (1984), An association between discrete aurora and energetic particle boundaries, *J. Geophys. Res.*, *89*, 2395–2400.

Lyons, L. R., and T. W. Speiser (1982), Evidence for current sheet acceleration in the geomagnetic tail, *J. Geophys. Res.*, *87*, 2276–2286.

Mende, S. B., et al. (2000), Far ultraviolet imaging from the IMAGE spacecraft, *Space Sci. Rev.*, *91*, 243–318.

Möbius, E., F. M. Ipavich, M. Scholer, G. Gloeckler, D. Hovestadt, and B. Klecker (1980), Observations of a nonthermal ion layer at the plasma sheet boundary during substorm recovery, *J. Geophys. Res.*, *85*, 5143–5148.

Parks, G. K., et al. (1984), Particle and field characteristics of the high-latitude plasma sheet boundary layer, *J. Geophys. Res.*, *89*, 8885–8906.

Parks, G., L. J. Chen, M. McCarthy, D. Larson, R. P. Lin, T. Phan, H. Rème, and T. Sanderson (1998), New observations of ion beams in the plasma sheet boundary layer, *Geophys. Res. Lett.*, *25*, 3285–3288.

Quinn, J. M., and C. E. McIlwain (1979), Bouncing ion clusters in the Earth's magnetosphere, *J. Geophys. Res.*, *84*, 7365–7370.

Quinn, J. M., and D. J. Southwood (1982), Observations of parallel ion energization in the equatorial region, *J. Geophys. Res.*, *87*, 10,536–10,540.

Rème, H., et al. (2001), First multispacecraft ion measurements in and near the Earth's magnetosphere with the identical Cluster ion spectrometry (CIS) instrument, *Ann. Geophys.*, *19*, 1–52.

Sauvaud, J.-A., D. Popescu, D. C. Delcourt, G. K. Parks, M. Brittnacher, V. Sergeev, R. A. Kovrazhkin, T. Mukai, and S. Kokubun (1999), Sporadic plasma sheet ion injections into the high-altitude auroral bulge: Satellite observations, *J. Geophys. Res.*, *104*, 28,565–28,586.

Sergeev, V. A., T. I. Pulkkinen, and R. J. Pellinen (1996), Coupled-mode scenario for the magnetospheric dynamics, *J. Geophys. Res.*, *101*, 13,047–13,065.

Sergeev, V. A., et al. (2000), Plasma sheet ion injections into the auroral bulge: Correlative study of spacecraft and ground observations, *J. Geophys. Res.*, *105*, 18,465–18,481.

Speiser, T. W. (1967), Particle trajectories in model current sheets: 2. Applications to auroras using a geomagnetic tail model, *J. Geophys. Res.*, *72*, 3919–3932.

Spjeldvik, W. N., and T. A. Fritz (1981), Energetic ion and electron observations of the geomagnetic plasma sheet boundary layer: Three-dimensional results from ISEE 1, *J. Geophys. Res.*, *86*, 2480–2486.

Takahashi, K., and E. W. Hones Jr. (1988), ISEE 1 and 2 observations of ion distributions at the plasma sheet-tail lobe boundary, *J. Geophys. Res.*, *93*, 8558–8582.

Wilken, B., et al. (1995), First results from the RAPID imaging energetic particle spectrometer on board Cluster, *Ann. Geophys.*, *19*, 1355–1366.

Williams, D. (1981), Energetic ion beams at the edge of the plasma sheet: ISEE 1 observations plus a simple explanatory model, *J. Geophys. Res.*, *86*, 5507–5518.

Zelenyi, L. M., R. A. Kovrazhkin, and J. M. Bosqued (1990), Velocity-dispersed ion beams in the nightside auroral zone: AUREOL 3 observations, *J. Geophys. Res.*, *95*, 12,119–12,139.

E. Amata, IFSI/CNR, Istituto Fisica dello Spazio Interplanetario, Area della Ricerca Tor Vergata, 100 Via del Fosso del Cavaliere, I-00133 Roma, Italy. (amata@ifsi.rm.cnr.it)

J. M. Bosqued, I. Dandouras, C. Jacquey, A. Keiling, B. Lavraud, P. Louarn, T. Moreau, H. Rème, J.-A. Sauvaud, and C. Vallat, CESR-CNRS, 9 avenue du Colonel Roche, BP 4346, F-31028 Toulouse Cedex 4, France. (jean-michel.bosqued@cesr.fr; iannis.dandouras@cesr.fr; christian.jacquey@cesr.cnes.fr; andreas.keiling@cesr.fr; benoit.lavraud@cesr.fr; philippe.louarn@cesr.fr; moreau@cesr.fr; henri.reme@cesr.fr; sauvaud@cesr.fr; vallat@cesr.fr)

P. Daly, Postfach 20, Max-Planck-Institut fur Aeronomie, Max Planck Str. 1, Katlenburg-Lindau D-37189, Germany. (daly@linmpi.mpg.de)

C. P. Escoubet, Solar System Division, Space Science Dept., ESA/ESTEC, Postbus 299, 2200 AG Noordwijk, Netherlands. (philippe.escoubet@esa.int)

B. Klecker, MPI für Extraterrestrische Physik, Karl-Schwarzschild Str. 1, Postfach 1312, D-85741 Garching b. Munchen, Germany. (bek@mpe.mpg.de)

A. Korth, Max-Planck-Institut fur Aeronomie, Max-Planck Str. 2, Postfach 20, D-37191 Katlenburg-Lindau, Germany. (korth@linmpi.mpg.de)

R. Lundin, Swedish Institute of Space Physics, P.O. Box 812, S-981 28 Kiruna, Sweden. (rickard.lundin@irf.se)

M. McCarthy, University of Washington, Geophysics Program, ATG Bldg., Box 351650, Room 202, Seattle, WA 98195-1650, USA. (mccarthy@geophys.washington.edu)

E. Möbius, University of New Hampshire, Morse Hall, Room 407, Space Science Center-EOS, 39 College Road, Durham, NH 03824, USA. (eberhard.moebius@unh.edu)

G. K. Parks, Space Science Laboratory, University of California, Berkeley, CA 94720, USA. (parks@ssl.berkeley.edu)

V. Sergeev, Institute of Physics, St. Petersburg State University, Ulyanovskya 1, Petrodvoretz, St. Petersburg 198504, Russia. (victor@geo.phys.spbu.ru)

Q.-G. Zong, Boston University, Center for Space Physics, 725 Commonwealth Avenue, Boston, MA 02215, USA. (zong@bu.edu)